CrossMark

Facile Synthesis and Characterization of GO/ZnS Nanocomposite with Highly Efficient Photocatalytic Activity

Lingwei Li[1] · Shaolin Xue[1] · Pei Xie[1,2] · Hange Feng[1] · Xin Hou[1] · Zhiyuan Liu[1] · Zhuoting Xu[1] · Rujia Zou[1]

Abstract

ZnS nanowalls, microspheres and rice-shaped nanoparticles have been successfully grown on graphene oxide (GO) sheets by the hydrothermal method. The morphologies, structures, chemical compositions and optical properties of the as-synthesized GO/ZnS have been characterized by X-ray power diffraction, energy dispersive spectrometer, scanning electron microscope, Raman spectra, photoluminescence spectroscopy and ultraviolet–visible absorption spectroscopy. It was found that the concentration of CTAB and the reaction temperature were important in the formation of GO/ZnS microstructures. The photocatalytic activity of the as-synthesized GO/ZnS was investigated through the photocatalytic degradation of textile dyeing waste. Results showed that the catalytic activity of the GO/ZnS porous spheres to methyl orange and methylene blue is higher than those of other samples. The degradation rates of methyl orange and methylene blue by porous spheres in 50 min were 97.6 and 97.1%, respectively. This is mainly attributed to the large specific surface area of GO/ZnS porous spheres and high separation efficiency between photogenerated electron and hole pairs.

Graphical Abstract
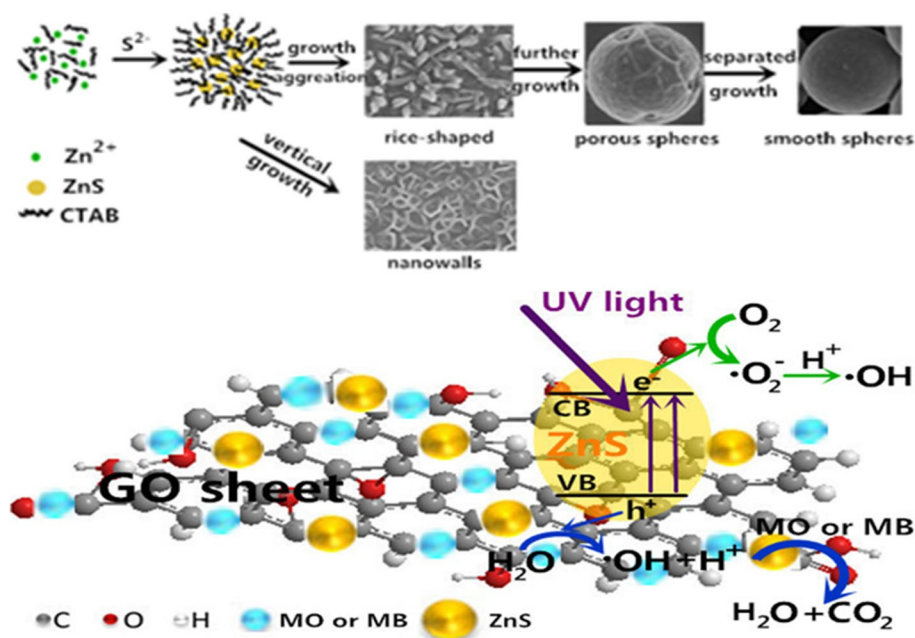
Extended author information available on the last page of the article

1 Introduction

Graphene, a single layer of sp^2-hybridized carbon atoms arranged in a two-dimensional hexagonal lattice, since 2004 was first discovered and has aroused great interest [1, 2]. Because the surface of GO has a large number of hydrophilic functional groups, GO has good solubility in water and can be interspersed. GO has become the first choice for many preparation of graphene based nanocomposites [3, 4]. In addition, GO has good electrical conductivity, great flexibility and good optical transparency, GO is also a potential material for electric, photonic and optoelectronic devices [5].

Zinc sulfide (ZnS) is an important II–VI group semiconductor compound with large direct wide band gap of 3.72–3.77 eV (3.72 eV for the cubic phase and 3.77 eV for the hexagonal wurtzite phase) and large exciton binding energy (40 meV), etc. [6–8]. Thanks to these excellent properties, ZnS is widely used in various high-tech applications, to name a few, light-emitting diode [9], sensors [10], infrared windows [11], photocatalysis [12], electroluminescent devices [13] and so on. In recent years, because the industry has developed rapidly, environmental pollution has become a major concern, especially water pollution which caused by the release of effluents and by waste dyes from the coloring industries. Therefore, an effective method is needed to degrade such toxic chemicals and waste dyes. It has been observed that photocatalytic degradation of organic dyes is one of the most effective ways to treat the water pollution [14–16]. In this respect, ZnS is considered one of the most effective photocatalyst degradation of organic pollutants. In the past few years, ZnS nano/micro-structures have been prepared by several preparation approaches including microemulsion method [17], solvothermal route [18], thermal decompose of precursor [19], hydrothermal method [20, 21] and solid–liquid chemical reaction [22]. ZnS nanocrystals with multiple morphologies, such as nanorods, nanowires [23, 24], nanobelts [23], whiskers [25], hollow nanospheres [26, 27], hollow nanovessels [28], nanostructure arrays [29, 30] and nanotubes [31, 32] have been synthesized and used for photocatalytic degradation of organic dyes and pigments [33, 34]. However, it is still a challenge to produce GO/ZnS composites in a facile and low-cost way for the degradation of waste dyes.

In this paper, by adjusting the concentration of CTAB and the reaction temperature, ZnS nanowalls, microspheres and rice-shaped nanoparticles have been successfully synthesized on graphene oxide sheets (GOss) by the hydrothermal method. The characterization and photocatalytic degradation applications of GO/ZnS were studied. Among the as-prepared samples, GO/ZnS porous spheres exhibited outstanding photodegradation efficiencies towards two dyes, i.e. methyl orange and methylene blue.

2 Experimental Procedure

2.1 Chemicals

All chemicals were of analytical grade and used as received without further purification. H_2SO_4 (98 wt.%), $KMnO_4$ (99.5 wt.%), H_2O_2 (30 wt.%), HCl (37 wt.%), graphite powder (GP), sodium nitrate ($NaNO_3$) (99.95 wt.%), Zinc acetate ($Zn(CH_3COO)_2 \cdot 2H_2O$) ($\geq$ 99.0%), cetyl trimethyl ammonium bromide (CTAB) ($\geq$ 99.0%) and sodium thiosulfate pentahydrate ($Na_2S_2O_3 \cdot 5H_2O$) ($\geq$ 97.0%). All aqueous solutions were prepared by using deionized water.

2.2 Synthesis of GO

Graphene oxide sheets were prepared from natural graphite by a modified Hummers method [35]. In short, 2 g of graphite powder and 2 g of sodium nitrate was dissolved in 40 mL of H_2SO_4 (98 wt.%) in a conical flask. The solution was stirred with a magnetic stirrer for 30 min in an ice-water bath. Then, 6 g of $KMnO_4$ (99.5 wt.%) was divided into 6 parts and added slowly to the mixed solution while the temperature was kept at 20 °C for 2 h and followed by stirring for 2 h at 35 °C. The mixed solution was diluted with 160 mL of deionized water and stirred intensely for 0.5 h at 90 °C. After that, 12 mL of H_2O_2 (30 wt.%) was slowly added to the solution and stirred thoroughly. The mixed solution was washed repeatedly with 0.5 mol/L HCl solution and deionized water to remove the residual sulfate ions. Lastly, GO was freeze-dried at − 60 °C under vacuum conditions. GO powder was obtained by grinding and used for the following experiments.

2.3 Synthesis of GO/ZnS

First, cut the silicon substrate into small pieces and clean it for about 30 min according to the steps of anhydrous ethanol, acetone, anhydrous ethanol and deionized water. At the same time, the GO powder was ultrasonically dispersed in anhydrous ethanol and stirred to form a uniform suspension. The uniform suspension was spin-coated on clean Si substrates. Finally, the silicon substrate is placed in a high temperature quartz furnace. Turn on the mechanical pump and start vacuuming, and then 100 sccm nitrogen gas is injected into the reaction chamber for 30 min. After that, set the temperature up to 650 °C within 1 h. When cooled to room temperature, graphene oxide sheets (GOss) can be formed on the surface of the silicon substrate.

In this experiment, ZnS grown on GOss were prepared by hydrothermal method. Firstly, 0.003 mol (0.659 g) $Zn(CH_3COO)_2 \cdot 2H_2O$ and 0.01 g of CTAB were dissolved in 40 mL of deionized water. The solution was stirred with a magnetic stirrer for 60 min. At the same time, 0.003 mol (0.745 g) $Na_2S_2O_3 \cdot 5H_2O$ were added into the solution mentioned above and the resulting solution was stirred thoroughly. After stirring, the final solution and GOss were put into a 100 mL autoclave and were hydrothermally processed for 16 h. The experimental conditions are shown in Table 1. After the solution was cooled down to room temperature, GOss were taken from the solution and washed repeatedly with deionized water and anhydrous ethanol to remove the unreacted chemicals [36, 37]. The final products were dried in a vacuum at 60 °C for 6 h. When the amount of CTAB is 0.01, 0.02, 0.04 g and the temperature is 120 °C, the products obtained are named as Sample 1, Sample 2 and Sample 3. The products obtained at 140, 160, 180 °C, and added amount of CTAB is 0.04 g are named as Sample 4, Sample 5, and Sample 6, respectively in Table 1.

2.4 Characterization

The crystalline phases of the as-prepared samples were characterized by X-ray power diffractometer (XRD; Rigaku D/max-2000) with Cu Kα ($\lambda = 1.5406$ Å) radiation operated at 40 kV and 200 mA in a 2θ range of 20–70°. The morphologies of the samples were analyzed by scanning electron microscope (SEM; Hitachi S-4800). The elements of the samples were examined by the energy dispersive spectroscope (EDS; Oxford IE 300X). The Raman spectra were measured using a dispersive Raman spectrometer (Jobin–Yvon XploRA). Room temperature photoluminescence (PL) measurements were recorded by the luminescence spectrometer (PL; Edinburgh FLS 920). Optical absorptions of the samples were recorded at room temperature using a UV–Vis spectrophotometer (UV–Vis; PerkinElmer Lambda 35).

3 Results and Discussion

3.1 X-Ray Diffraction Analysis (XRD)

Figure 1 shows the XRD pattern of ZnS nanowalls, microspheres and rice-shaped nanoparticles on GOss. All the samples exhibit similar XRD patterns, in which three peaks at 28.56°, 47.84° and 56.58° correspond to the three crystal planes of (111), (220) and (311) of cubic phase of ZnS (JCPDS card no. 79-0043), respectively. In the meantime, three weak diffraction peaks at $2\theta = 21.2, 24.5, 25.04$ are in agreement with the diffraction peak of GO [38], indicating that the ZnS grown on GOss. No diffraction from other crystalline forms was detected, indicating the high purity of the as-obtained GO/ZnS products. The narrowness and sharpness of the diffraction peaks reflected the good crystallinity of the as-synthesized GO/ZnS [39]. Moreover, with the increase of temperature, the full width at half maximum (FWHM) of diffraction peaks are becoming smaller, indicating the improving of crystallinity. The average crystallite sizes can roughly be estimated from the
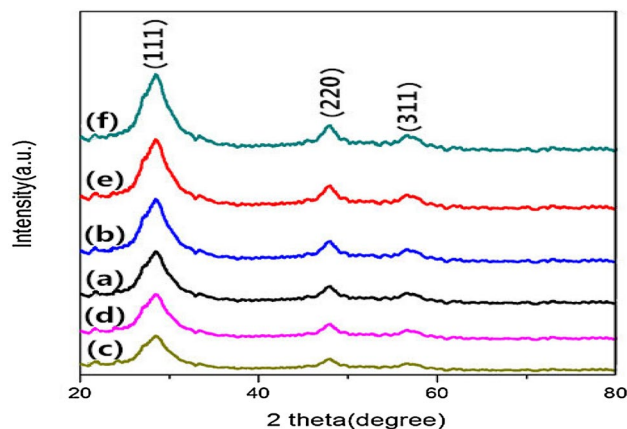

Fig. 1 XRD spectra of GO/ZnS obtained with different CTAB addition in solution **a** 0.01 g, **b** 0.02 g, **c** 0.04 g at 120 °C; SEM images of GO/ZnS obtained at different temperatures, **d** at 140 °C, **e** at 160 °C, **f** at 180 °C and the added amount of CTAB is 0.04 g

Table 1 The experimental conditions of all the samples

Sample	$Zn(CH_3COO)_2 \cdot 2H_2O$ (g)	Chelating agent (CTAB) (g)	$Na_2S_2O_3 \cdot 5H_2O$ (g)	T (°C)	t (h)
1	0.659	0.01	0.745	120	16
2	0.659	0.02	0.745	120	16
3	0.659	0.04	0.745	120	16
4	0.659	0.04	0.745	140	16
5	0.659	0.04	0.745	160	16
6	0.659	0.04	0.745	180	16

full width at half maxima (FWHM) of the (111) diffraction peak on the basis of the Scherrer formula:

$$D = 0.89\lambda / \beta \cos\theta \qquad (1)$$

where D is the average grain size, λ is the x-ray wavelength ($= 0.15406$ nm), θ is the (1 1 1) peak angle, and β is the full width at half maximum value. The average crystallite size of ZnS particles were about 2–4 μm.

3.2 Component Analysis

The chemical element composition of the GO/ZnS smooth microspheres (sample 6) is researched by X-ray energy dispersive spectroscope (EDS), and the spectrum is shown in Fig. 2. According to the calculation of the peak areas the molar ratio of the ZnS is 51.4/48.5, which is pretty close to the stoichiometric ratio of ZnS. Besides, the C and O signals are detected from the EDS spectrum, which come from GOss. As in the previous X-ray diffraction results, the result of EDS also reveals that ZnS grown on GOss. Also, no other impurity peaks detected in EDS spectra shows the high purity of the as-synthesized GO/ZnS [40, 41].

3.3 Morphological Analysis

Figure 3a–d show SEM images of the ZnS on GOss obtained at 120 °C and different CTAB concentrations. When CTAB addition is 0.01 g, the surface morphology of GO/ZnS nanowalls on GOss is shown in Fig. 3a. As shown in Fig. 3a, the width of the ZnS nanowalls is approximately 400–600 nm. With increasing CTAB to 0.02 g, ZnS rice-shaped nanoparticles were grown on GOss, as shown in Fig. 3b. Statistical analysis indicated that ZnS rice-shaped particles had a relatively narrow size distribution with an average diameter of about 200 nm and the average length of rice grains is about 600 nm. With the CTAB solution increasing to 0.04 g, ZnS
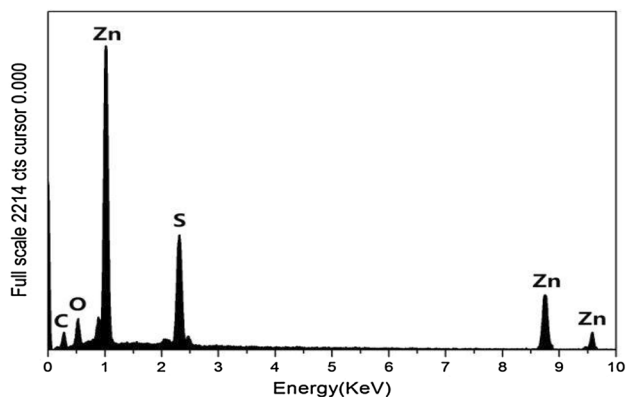

Fig. 2 EDS spectrum of ZnS smooth microspheres on GOss was prepared at a condition of 0.04 g of CTAB and a reaction temperature is 180 °C

porous spheres were grown on GOss, as shown in Fig. 3c. The average diameters of ZnS porous spheres are about 1 μm. It is observed that there are ZnS porous spheres on GOss, and the surface of porous spheres is not smooth and has many folds. And Fig. 3d is an enlarged figure of Fig. 3c. It can be found that the pore size is estimated to be 200 nm.

The above experimental results indicate that concentration of CTAB plays a key role in the formation of morphologies of as-synthesized ZnS microcrystals.

Figure 3e–h shows the SEM images of the products obtained at different hydrothermal temperatures with CTAB amount of 0.04 g. All the products exhibit sphere morphologies. Figure 3e is the SEM image of the product obtained at 140 °C. And Fig. 3e shows that the obtained samples consist of fews ZnS porous spheres with an average diameter of 800 nm and we can clearly observe GOss. Figure 3f is the higher magnification SEM image of Fig. 3e. It may be well observed that the wrinkling of ZnS porous spheres surface has been lost compared to the GO/ZnS sample obtained at 120 °C. Figure 3g is the SEM image of the samples obtained at 160 °C. GOss can be clearly observed from the images and the average diameters of ZnS spheres are about 2–3 μm. And the hole on the surface of the ZnS spheres disappears as the temperature increases, but the ZnS spheres are the same as the samples prepared at 120 and 140 °C with the presence of conglutination between the sphere and the sphere. When the temperature rises to 180 °C, we can clearly observe from Fig. 3h, the spheres size are almost not changed, the average diameters of the spheres are still 2–3 μm. However, there is no conglutination between the spheres, the dispersion is better, and the surface of the sphere is smooth.

The above experimental results show that the surface roughness of the obtained product decreases with the increase of temperature, and the dispersion has been gradually improved.

3.4 Raman Analysis

Raman spectroscopy is used to confirm the formation of ZnS phase structure and the existence of GO. Figure 4 shows a room temperature Raman spectra of ZnS smooth microspheres on Goss prepared at a condition of 0.04 g of CTAB and a reaction temperature of 180 °C (sample 6). As can be seen from the inset figure, strong peaks at 257 and 344 cm⁻¹ can be assigned as the TO and LO phonon modes of ZnS zinc blende structure, which is in good agreement with the reported results for ZnS nanotubes and hollow nanovessels [22, 23, 27, 28]. Besides, the two additional prominent peaks located at around 1340 and 1576 cm⁻¹ are attributed to the characteristic D band and G band of GO, which are ascribed to a breathing mode of κ-point photons of A_{1g} symmetry and the first order scattering of the E_{2g} phonon of sp² C atoms,

Fig. 3 SEM images of GO/ZnS obtained with different CTAB addition in solution **a** 0.01 g, **b** 0.02 g, **c** 0.04 g at 120 °C; SEM images of GO/ZnS obtained at different temperatures, **e** at 140 °C, **g** at 160 °C, **h** at 180 °C and the added amount of CTAB is 0.04 g
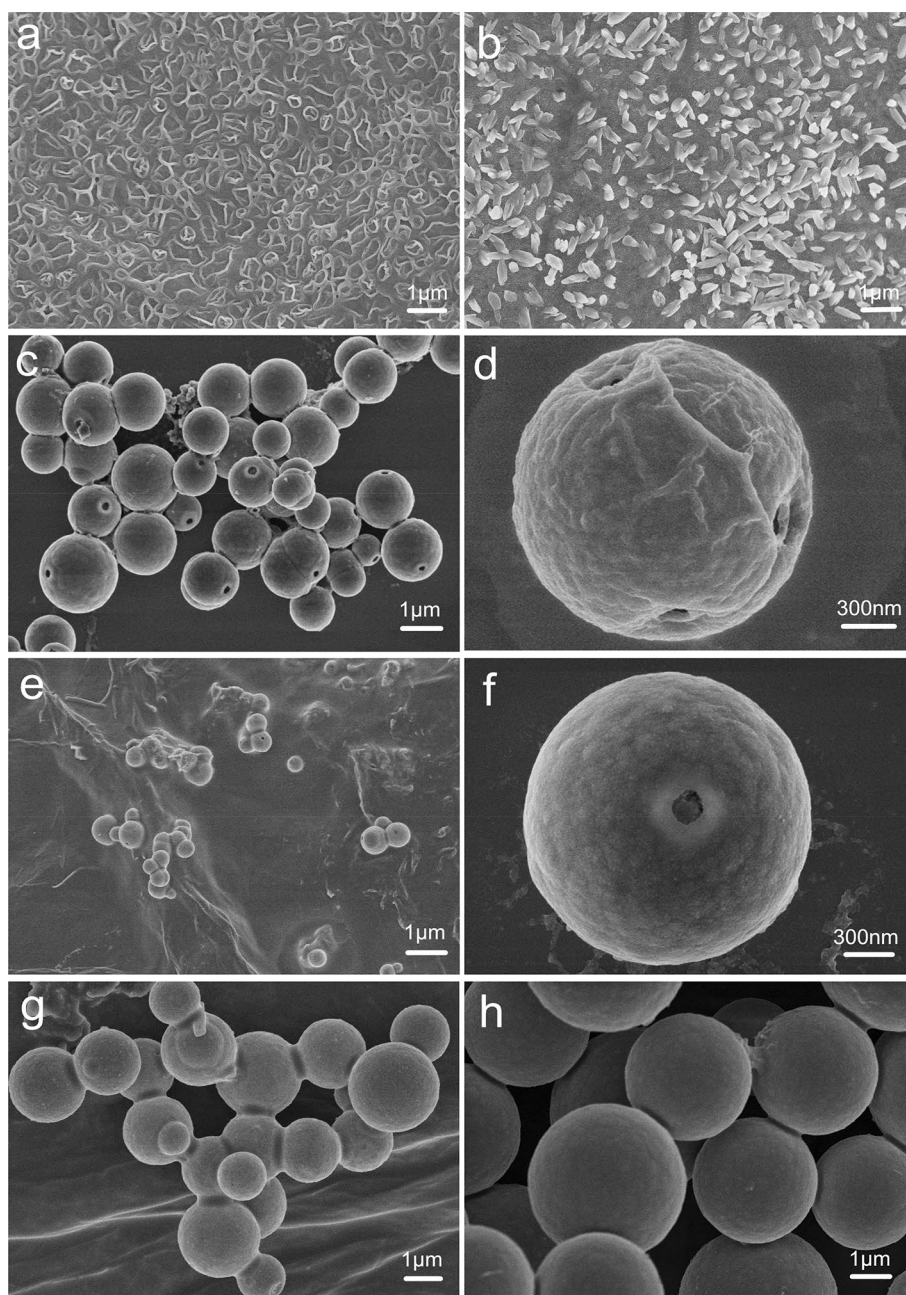
respectively [42]. All of the characteristics from Raman spectra indicated that ZnS microspheres are grown on Goss.

3.5 Optical Properties

The room temperature photoluminescence (PL) spectra of GO/ZnS products are shown in Fig. 5 (the excitation wavelength is 230 nm). From Fig. 5, GO/ZnS has two peaks, the peak near 360 nm is ZnS particle band edge absorption corresponding to the LUMO–HOMO (lowest unoccupied molecular orbital—highest occupied molecular orbital) as the electron transition. The other peak is located at about 462 nm, corresponding to the emission peak of the surface defect state of ZnS. The intensity of the fluorescence spectrum increases with the increase of defect density. The sample 3 has the highest intensity of PL emission, this is due to the fact that sample 3 contains more surface defects. The above results show that the optical properties of ZnS nanomaterials are very sensitive to specific reaction conditions. Obviously, the synthetic conditions, crystal size, and shape of the sample strongly affect the optical quality of ZnS semiconductor microcrystals [43, 44].

The UV–visible absorption spectrum of ZnS smooth microspheres on Goss is shown in Fig. 6. It can be seen from Fig. 6,
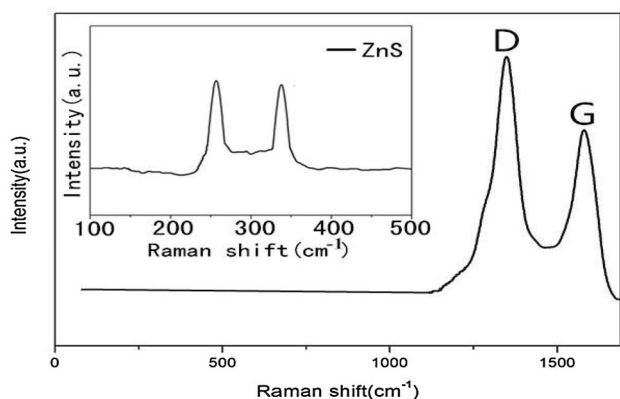
Fig. 4 Room temperature Raman spectra of ZnS smooth microspheres on Goss was prepared at a condition of 0.04 g of CTAB and a reaction temperature is 180 °C

Fig. 6 UV–Vis optical absorption spectrum of ZnS smooth microspheres on Goss was prepared at a condition of 0.04 g of CTAB and a reaction temperature is 180 °C

$$H^+ + S_2O_3^{2-} \rightarrow H_2S + SO_2 + SO_4^{2-} \tag{3}$$

$$Zn^{2+}/Zn(Ac)_2 + S^{2-}/H_2S \rightarrow ZnS + HAc \tag{4}$$

After adding surface active agent CTAB, Zn^{2+} ions in the reaction medium formed complex chelate with CTAB [46], as shown in the reaction (2). Sodium thiosulfate pentahydrate reacts in subacidity under the conditions of high temperature and pressure, as shown in reaction (3). The H_2S gas is generated and releasing S^{2-} ions. A stronger bond of conjugation between S^{2-} ions and Zn^{2+} ions causes Zn^{2+} ions to break away from the chelate complex CTAB-Zn^{2+} and form ZnS particle with S^{2-} ions, as shown in reaction (4). At the same time, the chelating action of surface active agent can effectively reduce the concentration of free Zn^{2+} ions in the solution and slow down the formation rate of ZnS particles, thus preventing the non-directional growth of excessive particles, resulting in irregular morphologies of the accumulation bodies.

The aggregation of these nanoparticles to microspheres may be driven by the solvent–polymer–nanoparticle surface interactions that change the mobility in solution finally inducing particles aggregation to form the Zn^{2+} ions covered complex spherical aggregates by minimization of energy [47]. Thus formed ZnS nanorods and provide nucleation centers for formation. When the concentration of CTAB increase in the above solution, more H_2S can be decomposed and many S^{2-} ions are released, then the nanorods grow in one direction and form the nanowalls perpendicular to the base, we can see from Fig. 3c. As the concentration of CTAB increases, the surface of the nanorods continues to aggregate S^{2-} ions and Zn^{2+} ions form the ZnS rice-shaped particles. When
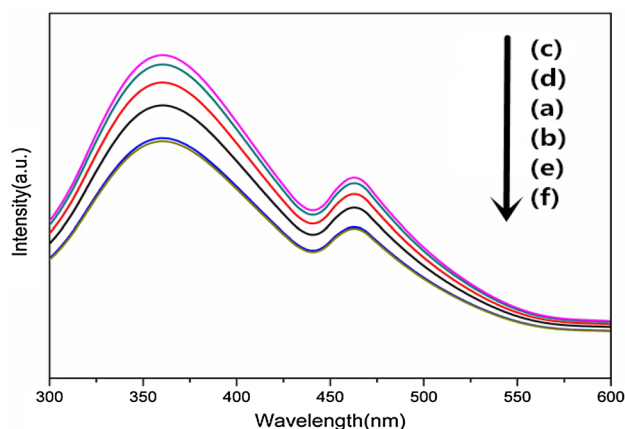

Fig. 5 Room temperature PL spectra of GO/ZnS obtained with different CTAB addition in solution **a** 0.01 g, **b** 0.02 g, **c** 0.04 g at 120 °C; SEM images of GO/ZnS obtained at different temperatures, **d** at 140 °C, **e** at 160 °C, **f** at 180 °C and the added amount of CTAB is 0.04 g

the absorption of ZnS microspheres for external and near ultraviolet light is remarkable. We can clearly find that GO/ZnS microspheres showed a strong absorption band, and the maximum absorption located at 323 nm. In addition, the weak absorption peak at 231 nm attributed to GOss [45], indicating that the ZnS microspheres were grown on Goss.

3.6 Mechanism

The possible mechanism can be illustrated in Scheme 1. In the hydrothermal environment, the concentration of CTAB and the reaction temperature play significant roles in the formation of ZnS microstructures. The mainly reactions in the process are shown as follows:
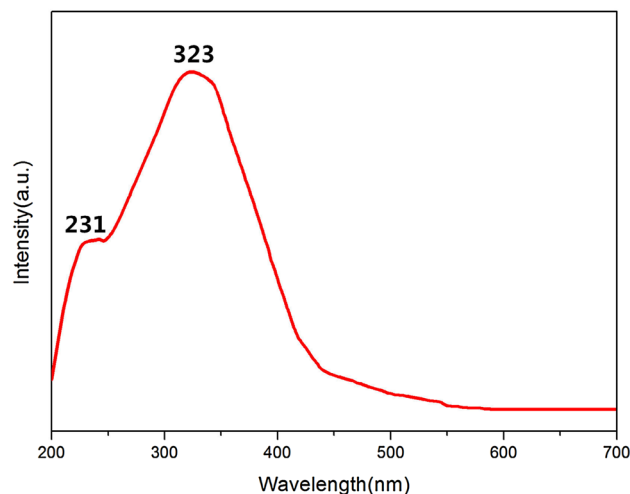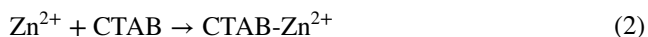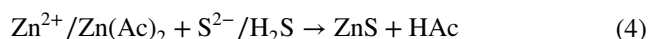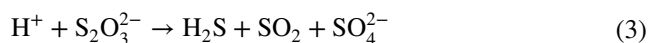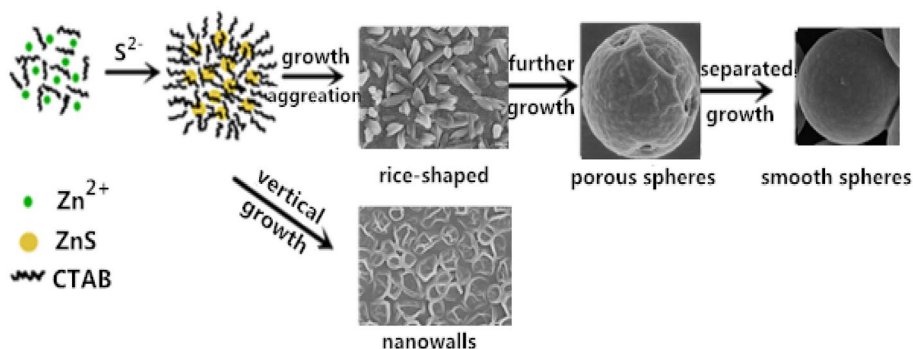
$$Zn^{2+} + CTAB \rightarrow CTAB\text{-}Zn^{2+} \tag{2}$$

Scheme 1 Schematic illustration of the formation mechanism of GO/ZnS

the concentration of CTAB in the above solution is high enough, the ZnS nanorods then nucleate, oriented grow up, and gathered on the surface of the Zn^{2+} ions covered aggregates. Finally, ZnS porous microspheres were formed. In addition, the increase in temperature can also promote Ostwald ripening, that is, the increase of voids and the decrease of shell thickness. At certain conditions, the porous spheres will break to form separated grains when the grain size and shell thickness reach a threshold, i.e., ZnS smooth microspheres [48].

3.7 Photocatalytic Performance of GO/ZnS

This paper chose the most representative organic pollutants in the printing and dyeing wastewater, methyl orange and methylene blue as targets for degradation. The photocatalytic degradation of methyl orange and methylene blue (50 mL; 20 mg/L) by GO/ZnS (20 mg) at room temperature and under UV light irradiation (8 W) was studied, and the following experimental results were obtained.

As shown in Fig. 7a, 20 mg/L methyl orange is irradiated by UV light for 50 min, the photocatalytic degradation efficiencies of GO/ZnS (S3) is 97.6%, much higher than those
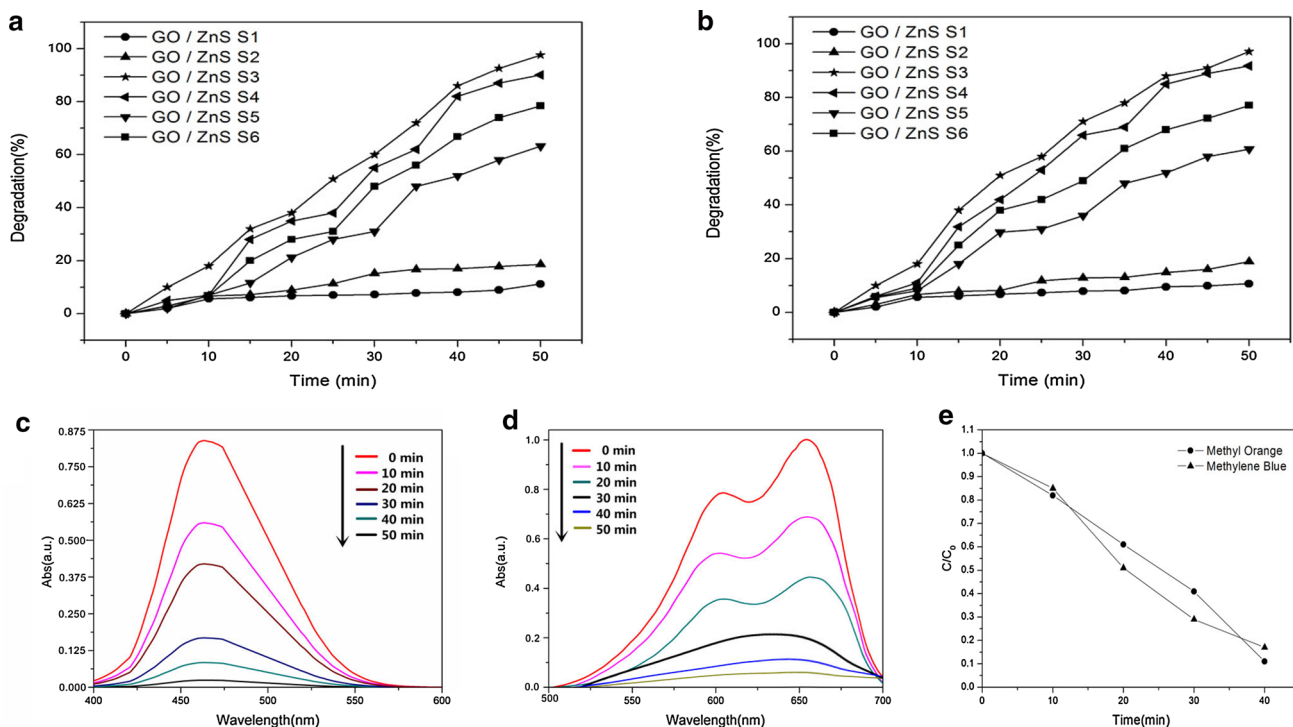

Fig. 7 a Photocatalytic degradation of methyl orange in the presence of different samples; **b** Photocatalytic degradation of methylene blue in the presence of different samples; **c** UV–Vis spectra of methyl orange after degraded by ZnS porous microspheres on GOss was prepared at a condition of 0.04 g of CTAB and a reaction temperature is 120 °C for different intervals; **d** UV–Vis spectra of methylene blue after degraded by ZnS porous microspheres on GOss was prepared at a condition of 0.04 g of CTAB and a reaction temperature is 120 °C for different intervals; **e** The photo degradation efficiencies of two dyes after 40 min illumination

of the GO/ZnS (S4) (90.1%), GO/ZnS (S6) (78.4%), GO/ZnS (S5) (63.2%), GO/ZnS (S2) (18.6%), and GO/ZnS (S1) (11.2%). It is easy to see that from Fig. 7b, 20 mg/L methylene blue is irradiated by UV light for 50 min, the photocatalytic degradation efficiency of GO/ZnS (S3) achieves 97.1% after 50 min. However, GO/ZnS (S4), GO/ZnS (S6), GO/ZnS (S5), GO/ZnS (S2) and GO/ZnS (S1) are only 89.7, 77.1, 60.8, 18.9 and 10.7%, respectively.

GO/ZnS (S3) shows higher catalytic activity for the methyl orange and methylene blue degradation compared to other samples. The excellent photocatalytic properties of GO/ZnS (S3) can be attributed to its surface wrinkles and porous structure. As is known to all, the photoreaction mainly proceeds on the surface of photocatalyst. The porous GO/ZnS (S3) can provide more reactive sites at the surface for adsorbing methyl orange and methylene blue. In addition, because the particle size of ZnS microspheres in the sample 3 is smaller, the photogenerated electron and hole pairs diffuse from the inside to the surface more quickly, the separation effect of photogenerated charge is higher and the recombination probability of electrons and holes is smaller. All above reasons enhance photocatalytic activity.

Figure 7c shows a time-dependent spectrum of methyl orange solution in the presence of 50 mg GO/ZnS microsphere (S3) under UV light irradiation. With the UV irradiation time increasing, the decrease in the intensity of absorbance peaks at 465 nm is attributed to photocatalytic degradation of methyl orange. An almost complete degradation was achieved in about 50 min. Figure 7d shows the absorption spectrum of an aqueous solution of methylene blue with 50 mg GO/ZnS microsphere (S3) under UV light irradiation for various durations. The absorption peaks corresponding to methylene blue decrease rapidly as the exposure time increases and almost completely disappear after 50 min. The slight blue-shift of absorption peaks with increase of exposure time could be attributed to a de-ethylated process of methylene blue in a stepwise manner [49]. No new absorption bands appeared in the whole spectrum, indicating the complete decomposition of methylene blue.

Figure 7e illustrates a comparison of the photocatalytic degradation efficiencies of methyl orange and methylene blue under the same experimental conditions. The changes of the organic pollutants concentrations under UV light irradiation are calculated as follows:

$$I = C/C_0 \times 100. \tag{5}$$

Among them, C_0 is the initial concentration of organic pollutants when the ultraviolet light is turned on. The real time concentration of organic pollutants under UV light irradiation is expressed by C. The photocatalytic efficiency of the organic dyes concentration change can be expressed by a relative ratio of C/C_0. The results showed that ZnS porous microspheres on GOss (S3) possess the high catalytic

efficiency towards methyl orange under our experimental conditions. GO/ZnS porous microsphere has different degradation properties to various dyes, the reason may be related to the molecular structure of dyes. Methyl orange contains easily degradable groups: –N=N– group. But methylene blue has different containing N groups, so the photocatalytic degradation efficiency is relatively low.

Scheme 2 illustrates the mechanism of photocatalytic degradation of organic dyes under UV irradiation. Based on the semiconductor excitation, the valence electrons of ZnS can be excited to the conduction band due to its narrow band gap, thus leaving holes in the valence band by absorbing ultraviolet light. When photogenerated electron and hole pairs migrate on the surface of the ZnS, the internal electric field passes through the semiconductor. The photogenerated electrons react with dissolved oxygen molecules and produce reactive oxygen radicals, and the photogenerated holes can react with the hydroxide ion derived from water to form hydroxyl radicals [50]. These peroxy radicals and hydroxyl radicals may cause methyl orange and methylene blue oxidation to decompose into CO_2, H_2O and other mineralized products, resulting in degradation effects. It should be pointed out that, although UV radiation can also directly decompose some organic dyes, the UV light power used in this study is very low and UV light cannot affect the overall photocatalytic degradation efficiency. In the present experiments, GO was added to the composite can enhance the photocatalytic degradation performance for two reasons [51–53]. One is because GO has a two-dimensional planar structure, so GO has good conductivity, thus, accomplishing the rapid transport of photogenerated carriers and achieving an effective charge separation. Another reason is that GO has a large specific surface area and is capable of adsorbing organic dye molecules. The surface of GO contains a large number of π-π conjugated double bonds. Consequently, oxygen radicals and hydroxyl radicals produced by GO/ZnS can degrade methyl orange and methylene blue dyes under UV light irradiation.
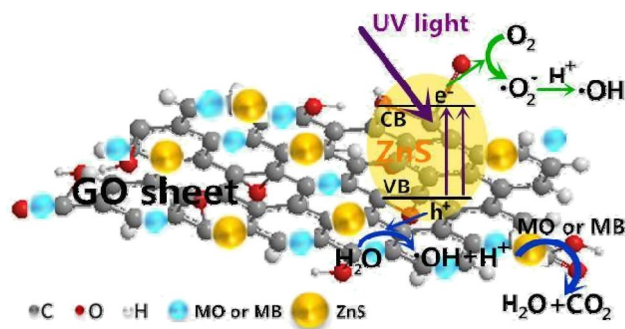
Scheme 2 Schematic for the degradation mechanism of methyl orange and methylene blue over GO/ZnS composites under light irradiation

4 Conclusions

In summary, ZnS nanowalls, microspheres and rice-shaped nanoparticles have been successfully grown on GOss by the hydrothermal method. The morphologies and size of the samples are influenced by the concentration of CTAB and the reaction temperature. When the concentration of CTAB increases, surface morphology of ZnS transforms nanowalls into rice-shaped ZnS nanoparticles and then becomes porous spheres. Besides, the surface roughness of the as-prepared samples decreases with the increase of reaction temperature, and the dispersity increases gradually. We find that low cost and environmental friendly properties of GO are reasonable to grow ZnS composites. When the amount of CTAB is 0.04 g and the reaction temperature is 120 °C, the as-prepared GO/ZnS porous microsphere has better catalytic performance compared to other samples, can degrade various dyes. The degradation rate of methyl orange reached 97.6% and the degradation rate of methylene blue was 97.1% in 50 min. This is mainly attributed to GO/ZnS porous microspheres with large specific surface area and an efficient charge separation. GO/ZnS porous microspheres are a potential material used in degrading textile dyeing waste.

Compliance with Ethical Standards

Conflict of interest We declare that they have no conflict of interest.

References

1. Geim, A.K., Novoselov, K.S.: The rise of graphene. Nat. Mater. **6**, 183–191 (2007)
2. Mahdiani, M., Sobhani, A., Salavati-Niasari, M.: Enhancement of magnetic, electrochemical and photocatalytic properties of lead hexaferrites with coating graphene and CNT: Sol-gel auto-combustion synthesis by valine. Sep. Purif. Technol. **185**, 140–148 (2017)
3. Fu, X., Bei, F., Wang, X., Brien, S.O., Lombardi, J.R.: Excitation profile of surface-enhanced Raman scattering in graphene-metal nanoparticle based derivatives. Nanoscale **2**, 1461–1466 (2010)
4. Song, H.S., Yang, C., Liu, D.B.: Dielectric properties of graphene/epoxy composites. J. Funct. Mater. **43**, 1185–1188 (2012)
5. Zhou, W.K., Xue, S.L., Han, J.W., Xie, P.: Synthesis of grass-like ZnSe nanostructures on graphene oxide and their excellent field eminssion properties. Mater. Lett. **134**, 256–258 (2014)
6. Ho, C.H.: Enhanced photoelectric-conversion yield in niobium incorporated In2S3 with intermediate band. J. Mater. Chem. **218**, 10518–10524 (2011)
7. Fang, X.S., Zhai, T.Y., Gautam, U.K., Li, L., Wu, L.M., Bando, Y., Golberg, D.: ZnS nanostructures: from synthesis to applications. Prog. Mater Sci. **56**, 175–287 (2011)
8. Jia, W.N., Wu, X., Jia, B.X., Qu, F.Y., Fan, H.J.: Self-Assembled porous ZnS nanospheres with high photocatalytic performance. Sci. Adv. Mater. **5**, 1329–1336 (2013)
9. Jia, W., Jia, B., Wu, X., Qu, F.Y.: Self-assembly of shape-controlled ZnS nanostructures with novel yellow light photoluminescence and excellent hydrophobic properties. Cryst. Eng. Comm. **14**, 7759–7763 (2012)
10. Fang, X.S., Bando, Y., Liao, M.Y., Zhai, T.Y., Gautam, U.K., Li, L., Koide, Y., Golberg, D.: An efficient way to assemble ZnS nanobelts as ultraviolet-light sensors with enhanced photocurrent and stability. Adv. Func. Mater. **20**, 500–508 (2010)
11. Liang, Y., Xu, H.Y., Hark, S.K.: Orientation and structure controllable epitaxial growth of ZnS nanowire arrays on GaAs substrates. J. Phys. Chem. C **114**, 8343–8347 (2010)
12. Pal, B., Pal, B.: Tuning the optical and photocatalytic properties of anisotropic ZnS nanostructures for the selective reduction of nitroaromatics. Chem. Eng. J. **263**, 200–208 (2015)
13. Kavanagh, Y., Alam, M.J., Cameron, D.C.: The characteristics of thin film electroluminescent displays produced using sol-gel produced tantalum pentoxide and Zinc Sulfide. Thin Solid Films **447–448**, 85–89 (2004)
14. Jia, B., Jia, W., Qu, F., Wu, X.: General strategy for self-assembly of mesoporous SnO2 nanospheres and their applications in water purification. RSC Adv. **3**, 2140–12148 (2013)
15. Liu, Y., Jiao, Y., Zhang, Z.L., Qu, F.Y., Umar, A., Wu, X.: Hierarchical SnO2 nanostructures made of intermingled ultrathin nanosheets for environmental remediation, smart gas sensor and supercapacitor applications. ACS Appl. Mater. Interfaces. **6**, 2174–2184 (2014)
16. Jiao, Y., Liu, Y., Yin, B., Zhang, S., Qu, F., Wu, X.: Hybrid α-Fe2O3@NiO heterostructures for flexible and high performance supercapacitor electrodes and visible light driven photocatalysts. Nano Energy **10**, 90–98 (2014)
17. Calandra, P., Longo, A., Liveri, V.T.: Synthesis of ultra-small ZnS nanoparticles by solid–solid reaction in the confined space of AOT reversed micelles. J. Phys. Chem. B **107**, 25–30 (2003)
18. Biswas, S., Kar, S.: Fabrication of ZnS nanoparticles and nanorods with cubic and hexagonal crystal structures: a simple solvothermal approach. Nanotechnology **19**, 045710 (2008)
19. Salavati-Niasari, M., Davar, F., Loghman-Estarki, M.R.: Controllable synthesis of thioglycolic acid capped ZnS(Pn)0.5 nanotubes via simple aqueous solution route at low temperatrures and conversion to wurtzite ZnS nanorods via thermal decompose of precursor. J. Alloys Compd. **494**, 199–204 (2010)
20. Salavati-Niasari, M., Davar, F., Seyghalkar, H., Esmaeili, E., Mir, N.: Novel inorganic precursor in the controlled synthesis of zinc blend ZnS nanoparticles via TGA-assisted hydrothermal method. Cryst. Eng. Comm. **13**, 2948–2954 (2011)
21. Salavati-Niasari, M., Davar, F., Mazaheri, M.: Synthesis and characterization of ZnS nanoclusters via hydrothermal processing from [bis (salicylidene) zinc (II)]. J. Alloys Compd. **470**, 502–506 (2009)
22. She, Y.Y., Yang, J., Qiu, K.Q.: Synthesis of ZnS nanoparticles by solid-liquid chemical reaction with ZnO and Na2S under ultrasonic. Trans. Nonferrous Metals Soc. China **20**, 211–215 (2010)
23. Fang, X.S., Ye, C.H., Zhang, L.D., Wang, Y.H., Wu, Y.C.: Temperature-controlled catalytic growth of ZnS nanostructures by the evaporation of ZnS nanopowders. Adv. Func. Mater. **15**, 63–68 (2005)
24. Park, S., Jin, C., Kim, H., Hong, C., Lee, C.: Enhanced violet emission from ZnS nanowires annealed in an oxygen atmosphere. J. Lumin. **132**, 231–235 (2012)
25. Fang, X.S., Bando, Y.S., Ye, C.H., Shen, G.Z., Golberg, D.: Shape-and size-controlled growth of ZnS nanostructures. J. Phys. Chem. C **111**, 8469–8474 (2007)

26. Ma, Y.R., Qin, L.M., Ma, J., Cheng, H.: Facile synthesis of hollow ZnS nanospheres in block copolymer solutions. Langmuir **19**, 4040–4042 (2003)

27. Bi, C., Pan, L.Q., Guo, Z.G., Zhao, Y.L., Huang, M.F., Ju, X., Xiao, J.Q.: Facile fabrication of wurtzite ZnS hollow nanospheres using polystyrene spheres as templates. Mater. Lett. **64**, 1681–1683 (2010)

28. Chen, X.J., Xu, H.F., Xu, N.S., Zhao, F.H., Lin, W.J., Lin, G., Fu, Y.L., Huang, Z.L., Wang, H.Z., Wu, M.M.: Kinetically controlled synthesis of wurtzite ZnS nanorods through mild thermolysis of a covalent organic-inorganic network. Inorg. Chem. **42**, 3100–3106 (2003)

29. Fang, X.S., Wu, L.M., Hu, L.F.: ZnS nanostructure arrays: a developing material star. Adv. Mater. **23**, 585–598 (2011)

30. Fang, X.S., Bando, Y., Ye, C.H., Golberg, D.: Crystal orientation-ordered ZnS nanobelt quasi-arrays and their enhanced field-emission. Chem. Commun. **29**, 3048–3050 (2007)

31. Yin, L.W., Bando, Y., Zhan, J.H., Li, M.S., Golberg, D.: Self-assembled highly faceted wurtzite-type ZnS single-crystalline nanotubes with hexagonal cross-sections. Adv. Mater. **17**, 1972–1977 (2005)

32. Shao, H.F., Qian, X.F., Huang, B.C.: Fabrication of single-crystal ZnO nanorods and ZnS nanotubes through a simple ultrasonic chemical solution method. Mater. Lett. **61**, 3639–3643 (2007)

33. Guo, C.F., Zhang, J., Wang, M., Tian, Y., Liu, Q.: A strategy to prepare wafer scale bismuth compound superstructures. Small **9**, 2394–2398 (2013)

34. Guo, C.F., Lan, Y.C., Sun, T.Y., Ren, Z.F.: Deformation-induced cold-welding for self-healing of super-durable flexible transparent electrodes. Nano Energy **8**, 110–117 (2014)

35. Zou, R.J., He, G.J., Xu, K.B., Liu, Q., Zhang, Z.Y., Hu, J.Q.: ZnO nanorods on reduced graphene sheets with excellent field emission, gas sensor and photocatalytic properties. J. Mater. Chem. A **1**, 8445–8452 (2013)

36. Sobhani, A., Salavati-Niasari, M.: Cobalt selenide nanostructures: hydrothermal synthesis, considering the magnetic property and effect of the different synthesis conditions. J. Mol. Liq. **219**, 1089–1094 (2016)

37. Sobhani, A., Salavati-Niasari, M.: Morphological control of $MnSe_2/Se$ nanocomposites by amount of hydrazine through a hydrothermal process. Mater. Res. Bull. **48**, 3204–3210 (2013)

38. Gadzuk, J.W., Plummer, E.W.: Field emission energy distribution. Rev. Mod. Phys. **45**, 487–548 (1973)

39. Sobhani, A., Salavati-Niasari, M.: Single-source molecular precursor for synthesis of CdS nanoparticles and nanoflowers. High Temp. Mater. Processes **31**, 157–162 (2012)

40. Sobhani, A., Salavati-Niasari, M.: Hydrothermal synthesis of CoSe nanostructures without using surfactant. J. Mol. Liq. **220**, 334–338 (2016)

41. Sobhani, A., Salavati-Niasari, M.: Chromium selenide nanoparticles: hydrothermal synthesis in the presence of a new selenium source. J. Nanostruct **7**, 141–146 (2017)

42. Song, P., Zhang, X.Y., Sun, M.X., Cui, X.L., Lin, Y.H.: Synthesis of graphene nanosheets via oxalic acid-induced chemical reduction of exfoliated graphite oxide. RSC Adv. **2**, 1168–1173 (2012)

43. Geng, J., Liu, B., Xu, L., Hu, F.N., Zhu, J.J.: Facile route to Zn-based II–VI semiconductor spheres, hollow spheres, and core/shell nanocrystals and their optical properties. Langmuir **23**, 10286–10293 (2007)

44. Sobhani, A., Salavati-Niasari, M.: Optimized synthesis of ZnSe nanocrystals by hydrothermal method. J. Mater. Sci.: Mater. Electron. **27**, 293–303 (2016)

45. Srivastava, M., Uddin, M.E., Singh, J., Kim, N.H., Lee, J.H.: Preparation and characterization of self-assembled layer by $NiCo_2O_4$-reduced graphene oxide nanocomposite with improved elecatalytic properties. J. Alloys. Compd. **590**, 266–276 (2014)

46. Sobhani, A., Salavati-Niasari, M.: CdSe nanoparticles: facile hydrothermal synthesis, characterization and optical properties. J. Mater. Sci.: Mater. Electron. **26**, 6831–6836 (2015)

47. Panda, S.K., Datta, A., Chaudhuri, S.: Nearly monodispersed ZnS nanospheres: synthesis and optical properties. Chem. Phys. Lett. **440**, 235–238 (2007)

48. Yan, Q., Wu, A.P., Yan, H.J., Dong, Y.Y., Tian, C.G., Jiang, B.J., Fu, H.G.: Gelatin-assisted synthesis of ZnS hollow nanospheres: the microstructure tuning, formation mechanism and application for Pt-free photocatalytic hydrogen production. Cryst. Eng. Comm. **19**, 461 (2017)

49. Watanabe, T., Takizawa, T., Honda, K.: Photocatalysis through excitation of adsorbates. 1. Highly efficient N-deethylation of rhodamine B adsorbed to cadmium sulfide. J. Phys. Chem. **81**, 1845–1851 (1977)

50. Qin, Y.L., Sun, Z., Zhao, W.W., Liu, Z.Y., Ni, D.R., Ma, Z.Y.: Effect of S^{2-} donors on synthesizing and photocatalytic degrading properties of ZnS/RGO nanocomposite. Appl. Phys. A **123**, 355 (2017)

51. An, X.Q., Yu, J.C.: Graphene-based photocatalytic composites. RSC Adv. **1**, 1426–1434 (2011)

52. Zhang, H., Lv, X.J., Li, Y.M., Wang, Y., Li, J.H.: P25-graphene composite as a high performance photocatalyst. ACS Nano **4**, 380–386 (2010)

53. Lee, J.S., You, K.H., Park, C.B.: Highly photoactive, low band-gap TiO_2 nanoparticles wrapped by graphene. Adv. Mater. **24**, 1084–1088 (2012)

Affiliations

Lingwei Li[1] · Shaolin Xue[1] · Pei Xie[1,2] · Hange Feng[1] · Xin Hou[1] · Zhiyuan Liu[1] · Zhuoting Xu[1] · Rujia Zou[1]

✉ Shaolin Xue
slxue@dhu.edu.cn

Lingwei Li
li.lingwei.pink@163.com

Pei Xie
peipeixie@163.com

Hange Feng
17721486315@163.com

Xin Hou
Houxin2016@163.com

Zhiyuan Liu
l1085644418@163.com

Zhuoting Xu
zhuotingxu@163.com

Rujia Zou
rujiazou@163.com

[1] College of Science, Donghua University, Shanghai 201620, China

[2] School of Information Science and Technology, Donghua University, Shanghai 201620, China